

# SLE description of the nodal lines of random wave functions

**E. Bogomolny, R. Dubertrand, and C. Schmit**

CNRS, Université Paris-Sud, UMR 8626,  
Laboratoire de Physique Théorique et Modèles Statistiques, 91405 Orsay, France

E-mail: [remy.dubertrand@lptms.u-psud.fr](mailto:remy.dubertrand@lptms.u-psud.fr)

**Abstract.** The nodal lines of random wave functions are investigated. We demonstrate numerically that they are well approximated by the so-called  $SLE_6$  curves which describe the continuum limit of the percolation cluster boundaries. This result gives an additional support to the recent conjecture that the nodal domains of random (and chaotic) wave functions in the semi classical limit are adequately described by the critical percolation theory. It is also shown that using the dipolar variant of SLE reduces significantly finite size effects.

PACS numbers: 05.45.Mt, 03.65.Sq, 64.60.Ak

## 1. Introduction

In 1977 Berry conjectured [1] that the wave functions of chaotic quantum systems can statistically be described by Gaussian random functions with a spectrum computed from the ergodic average.

For example, the wave functions for two-dimensional billiards without magnetic field  $\Psi(\vec{x})$  have to obey the equation

$$(\Delta + k^2)\Psi(\vec{x}) = 0 \tag{1}$$

and, say, the Dirichlet boundary conditions.

From general considerations it follows that such functions can be represented as a formal sum over elementary solutions of (1) e.g.

$$\Psi(r, \theta) = \sum_{m=-\infty}^{\infty} C_m J_{|m|}(kr) e^{im\theta} \tag{2}$$

where  $J_m(x)$  are usual Bessel functions and  $C_{-m} = C_m^*$ .

The Berry conjecture signifies that for chaotic billiards like the stadium billiard, real and imaginary parts of coefficients  $C_m$  with non-negative  $m$  are independent identically distributed Gaussian random variables with zero mean and variance computed from the normalization.

The beauty of this profound conjecture lies first of all in its simplicity and generality. On the other hand, it represents chaotic wave functions as completely structureless and 'uninteresting' objects which to some extent was the reason of relatively few investigations of the chaotic wave functions.

In 2002 Smilansky *et al.* [2] stimulated a renewal of interest in this problem. Instead of considering the coefficients of an expansion as in (2) these authors looked for the nodal domains of wave functions, i.e. the regions where a function has a definite sign. They have also observed that for chaotic wave functions the nodal domains have a rich unexpected structure worth investigating in details.

In [3] on physical grounds it was conjectured that the nodal domains of random wave functions (and, consequently, of chaotic wave functions) can be adequately described by a critical percolation model (see e.g. [6]). Due to the universality of the critical percolation it is unessential what special percolation model is considered. All of them lead to the same critical exponents as well as to other universal quantities. In [3] it was checked numerically that many predictions of the critical percolation model, such as the number of connected domains, their area distribution, cluster fractal dimensions etc. agree very well with corresponding quantities computed from the nodal domains of random (and chaotic) wave functions. In [4] it was demonstrated that the level domains (the regions where a function is bigger than a certain non-zero value) are well described by a non-critical percolation model. These and other investigations strongly suggest that the critical percolation model is applicable for the description of the nodal domains of random and chaotic wave functions. Though it sounds physically quite natural and can

be confirmed by a careful application of Harris' criterion [4], a rigorous mathematical proof was not yet found and further numerical verifications are desirable.

The purpose of this paper is to check another prediction of the percolation model namely that the boundaries of the percolation clusters are described by what is called  $\text{SLE}_6$  curves (see below). This statement was proved in 2001 for the critical percolation on the triangular lattice by Smirnov [7] and it is widely accepted that it remains true for all critical percolation models. For the nodal domains of random functions it leads to the conclusion that the nodal lines (curves where a function is zero) have to be also described by  $\text{SLE}_6$  curves.

The plan of the paper is the following. In section 2 for completeness we give an informal introduction to the SLE curves. This name is attributed to two-dimensional self-avoiding curves generated by an one-dimensional Brownian motion with zero mean and the variance linear in time with a coefficient of proportionality equal to a real positive number  $\kappa$ . In 2000 Schramm proved that if the different parts of a random self-avoiding curve are independent and the curve itself is in a certain sense conformally invariant then it belongs to SLE curves with a certain value of  $\kappa$ . Smirnov's result [7] means that the percolation boundaries are generated by the Brownian motion with  $\kappa = 6$ . In section 3 we present the results of direct numerical calculations of corresponding Brownian-like generating curves for the nodal lines of random wave functions and found that they are well described by  $\text{SLE}_6$ . The inevitable drawback of numerical calculations is that one always deals with curves of finite size. But the theorem about the relation between the percolation boundaries and  $\text{SLE}_6$  is valid only for infinite curves. To decrease such a finite size effect we use in section 4 a different version of SLE called dipolar SLE [10]. In this approach one first conformally transforms a given region into, say, an infinite band and then uses a suitably modified SLE equation. By this method we numerically demonstrate that the nodal lines of random wave functions agree well with the  $\text{SLE}_6$  description thus once more confirming the conjectural relation between the critical percolation and the nodal domains of random wave functions. In the appendix the numerical algorithms used in calculations are shortly discussed.

To a certain degree our work was stimulated by [5] where it was numerically checked that the nodal lines of the vorticity field in two-dimensional turbulence are close to  $\text{SLE}_6$  curves. In the recent publication [11] Keating, Marklof and Williams have demonstrated that the nodal lines for a perturbed cat map are well described by  $\text{SLE}_6$ . They also performed [12] numerical calculations for the nodal lines of random wave functions which lead to the same conclusions. Our results are in complete agreement with their findings.

## 2. Schramm-Loewner Evolution

Two-dimensional self-avoiding curves appear naturally in many physically important problems. But analytically imposing the condition of self-avoiding is not simple. In 1923 Loewner proposed [8] to describe such curves by conformal transformations which map a domain with a simple curve growing from the boundary to another simply connected

domain without the curve. In the simplest setting one considers the upper half plane  $\mathbb{H}$  with a simple curve  $\mathcal{C}$  and looks for a conformal map which transforms the upper half plane minus the curve,  $\mathbb{H} \setminus \mathcal{C}$ , to  $\mathbb{H}$  itself (see figure 1).

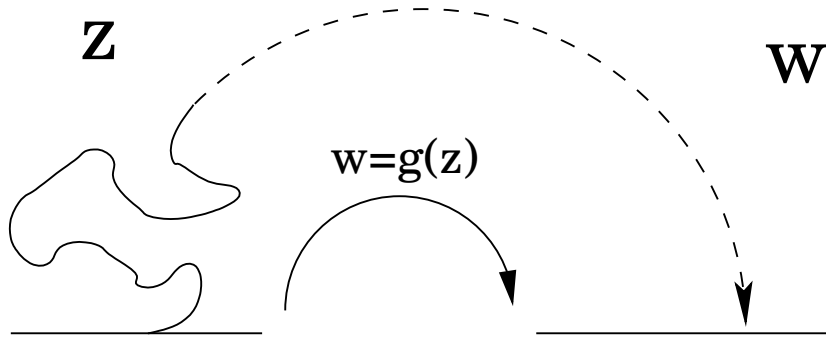


**Figure 1.** Loewner’s evolution. The upper half plane of the variable  $z$  with a cutoff along a simple curve is transformed by a conformal map  $w = g(z)$  to the whole upper half plane of the variable  $w$ .

The main point of this approach is the well known Riemann theorem according to which any simply connected region can be conformally mapped to another simply connected region and, inversely, if one applies a conformal transformation to a simply connected region the result will be also a simply connected region.

Such conformal transformations are not unique and depend on 3 free parameters. For example, the upper half plane  $\mathbb{H}$  is transformed to itself by 3 parameter group of fractional transformations

$$g(z) = \frac{az + b}{cz + d} \tag{3}$$

with real  $a, b, c, d$ .

To fix uniquely the conformal map  $g(z)$  it is convenient to impose the so-called hydrodynamic normalization by fixing the behaviour of the map at infinity:

$$g(z) = z + \frac{2t}{z} + \dots \text{ when } |z| \rightarrow \infty . \tag{4}$$

Parameter  $t$  is a characteristic of the initial region called capacity. To stress its importance we shall denote the map  $g(z)$  with asymptotic (4) by  $g_t(z)$  showing explicitly the dependence of  $t$ . This quantity can be also called ‘conformal time’ as it fulfils the additivity property which follows directly from (4)

$$g_t(g_s) = g_{t+s} . \tag{5}$$

The simplest example of a curve is a vertical slit in the upper half plane. If  $(\xi, h)$  are coordinates of the top of the slit (see figure 2) the transformation

$$w(z) = \xi + \sqrt{(z - \xi)^2 + 4t} \tag{6}$$

with  $t = h^2/4$  maps the upper half plane of  $z$  with the slit to the upper half plane of  $w$  without the slit.

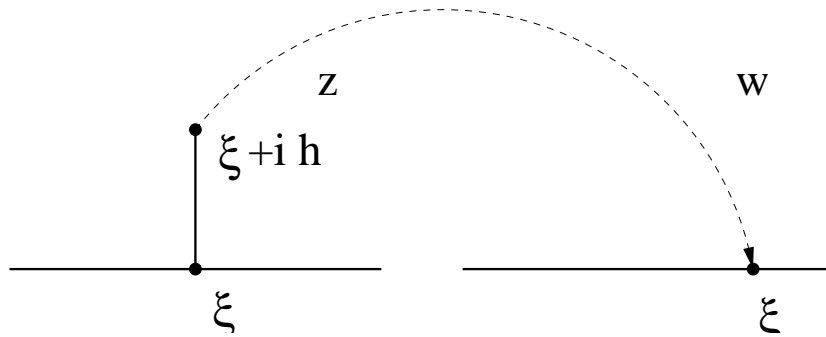


**Figure 2.** Transformation of a vertical slit to the upper half plane by map (6).

Interpreting  $t$  as the time permits to derive the equation for  $g_t(z)$ . From (5) it follows that

$$g_{t+\delta t}(z) = g_{\delta t}(g_t(z)) . \tag{7}$$

For small  $\delta t$  any line can approximately be considered as a vertical slit growing from the image of the tip of the curve under  $g_t$  which we denote by  $\xi_t$  (see appendix). Now (6) states that

$$g_{\delta t}(z) \xrightarrow{\delta t \rightarrow 0} z + \frac{2\delta t}{z - \xi_t} . \tag{8}$$

Combining two last equations one concludes that  $g_t(z)$  as function of  $t$  obeys the following differential equation called Loewner's equation

$$\frac{dg_t(z)}{dt} = \frac{2}{g_t(z) - \xi_t} \tag{9}$$

with initial condition

$$g_0(z) = z . \tag{10}$$

The function  $\xi_t$  is called the 'driving' or 'forcing' function. The curve itself is called the 'trace' and can be computed from the relation

$$z(t) = g_t^{-1}(\xi_t) . \tag{11}$$

The advantage of Loewner's equation (9) and (11) is that for any smooth (differentiable) function  $\xi_t$  it will produce a two-dimensional self-avoiding curve and, inversely, any self-avoiding curve will give a smooth function  $\xi_t$ .

The next important step was done by Schramm. In 2000 he proved [9] that random self-avoiding curves with the following properties:

- conformal invariance,
- statistical independence of different parts,
- reflection symmetry

are generated by the usual one-dimensional Brownian motion with zero mean and the variance linear in  $t$

$$\xi_t = \sqrt{\kappa} B_t, \quad \langle B_t \rangle = 0, \quad \langle B_t B_s \rangle = |t - s|. \quad (12)$$

Such curves only depend on one real positive parameter  $\kappa$  and are called stochastic (or Schramm) – Loewner evolution curves or shortly  $\text{SLE}_\kappa$ .

As Brownian curves are not differentiable,  $\text{SLE}_\kappa$  curves may have self-touching points. Depending on the value of  $\kappa$  they are divided into three phases (see e.g. [13]). For  $0 < \kappa \leq 4$  the traces are simple curves, for  $4 < \kappa < 8$  they can have double points or hit the real axis, and for  $\kappa \geq 8$  they fill the entire domain.

SLE is a very powerful tool to study rigorously the scaling (continuum) limit of different discrete models (see e.g. [13] and [14]). The most important for us is the Smirnov’s result [7]: the boundaries of clusters in the critical percolation (on a triangular lattice) converge in the continuum limit to the traces of  $\text{SLE}_6$ . As the nodal domains of random wave functions are conjectured to be described by critical percolation [3] it means that the nodal lines of random wave functions in this limit have to be also described by  $\text{SLE}_6$  curves. The verification of this statement is the main purpose of this work.

### 3. The nodal lines of random wave functions

The nodal lines are lines where a real function of two variables is zero,  $\Psi(x, y) = 0$ . They can, in principle, be computed numerically for any function  $\Psi(x, y)$ . For random wave functions (2) the nodal lines are quite complicated. An example of a nodal line is presented in figure 3. To demonstrate the complexity and self-avoiding character of such a curve, its small portion enclosed by a rectangle is enlarged in the inset of this figure.

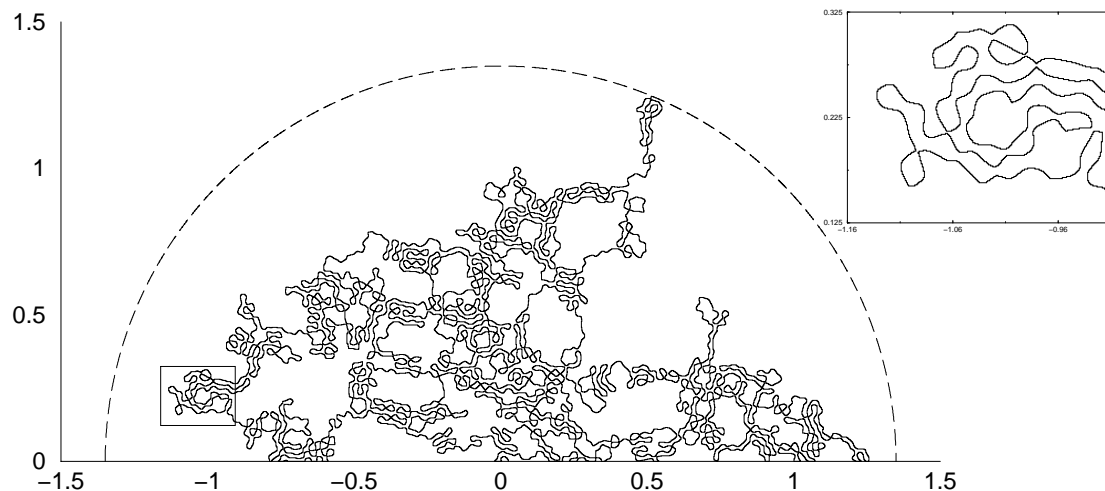


**Figure 3.** A nodal line of a random wave function. The dashed line indicates the absorbing half-circle. *Insert:* Magnification of the indicated rectangular region.

As all pictures of nodal lines are necessarily finite, one has to decide what to do with a nodal line which hits the boundary. There are two main types of boundaries: reflecting and absorbing. If a growing line touches a reflecting boundary it follows the boundary in the increasing direction till the next appearance of the sign change and then continues along a new nodal line. This can be achieved automatically by imposing the sign function outside the boundary. If a boundary is absorbing, one simply stops any line which hits it. In figure 3 the horizontal line is a reflecting boundary but the half-circle indicated by the dashed line is an absorbing one.

In general the properties of  $SLE_\kappa$  curves inside a region do depend on chosen boundary conditions. But for  $SLE_6$  lines it is proved (see e.g. [13]) that they feel the boundaries only when they hit them so the boundary conditions are unessential for the investigation of the local properties of the percolation cluster interfaces and, as conjectured, of the nodal lines of random wave functions.

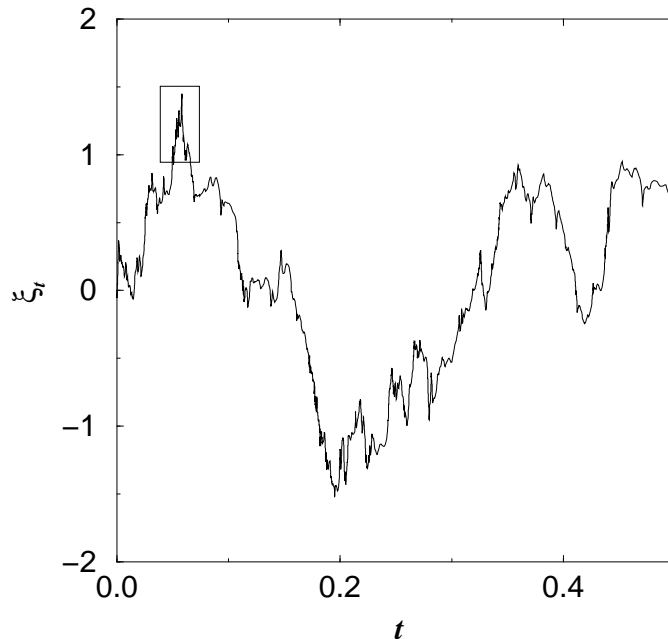


**Figure 4.** Forcing function corresponding to the nodal line of figure 3.

Having generated a line as in figure 3, the next step is to find the conformal map which transforms it to the upper half plane. There are many good algorithms which permit to do it numerically (see [15] and references therein). We used the so-called geodesic algorithm [15] in which a small segment of a line to be mapped is approximated by an arc of a geodesic circle perpendicular to the real axis and passing through the tip of the segment (see appendix). This algorithm is quite stable and is easy to implement.

In figure 4 we plot the forcing function which corresponds to the nodal line of figure 3 and in figure 5 fine details of this function are given.

We have numerically computed 2248 different realizations of the random wave function (2) with  $k = \sqrt{E} = 100$ . For each realization we have found the nodal lines which were stopped when they hit the half-circle as in figure 3.

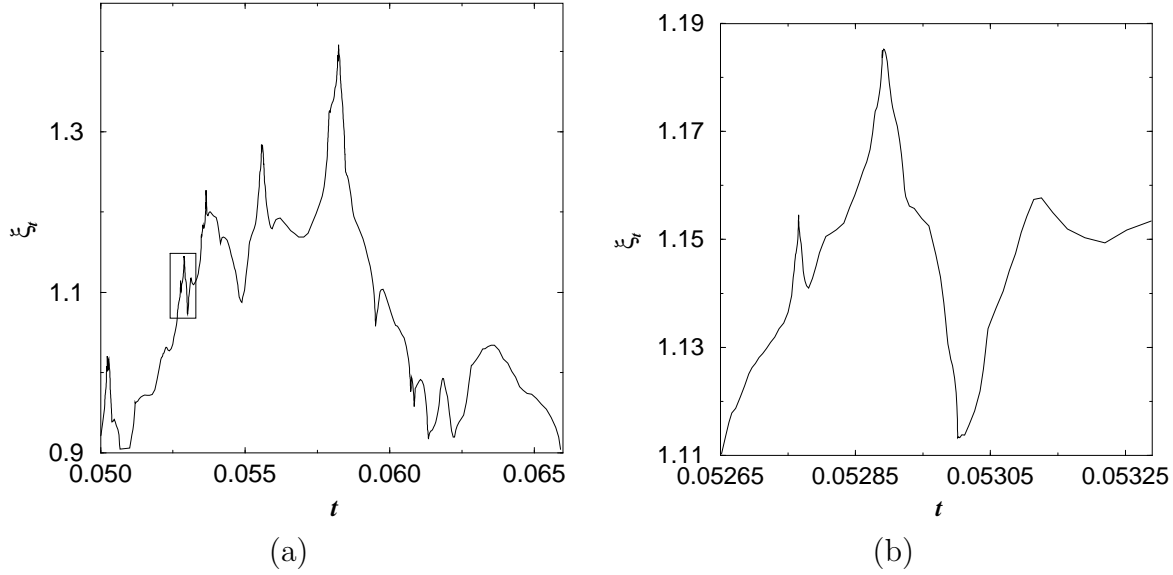


**Figure 5.** (a) Magnification of the small rectangular region in figure 4. (b) Magnification of the rectangular region in (a).

Then corresponding forcing functions,  $\xi_t(j)$ , were calculated using the geodesic algorithm. To check that these functions are well described by the Brownian curves we calculated mean value  $\bar{\xi}_t$  and variance  $\sigma^2(t)$  for each  $t$  from the usual relations

$$\bar{\xi}_t = \frac{1}{N} \sum_{j=1}^N \xi_t(j), \quad \sigma^2(t) = \frac{1}{N} \sum_{j=1}^N (\xi_t(j) - \bar{\xi}_t)^2. \quad (13)$$

In figure 6 the dependence  $\sigma^2(t)$  is plotted for all  $t$ . It is clearly seen that it is not linear.

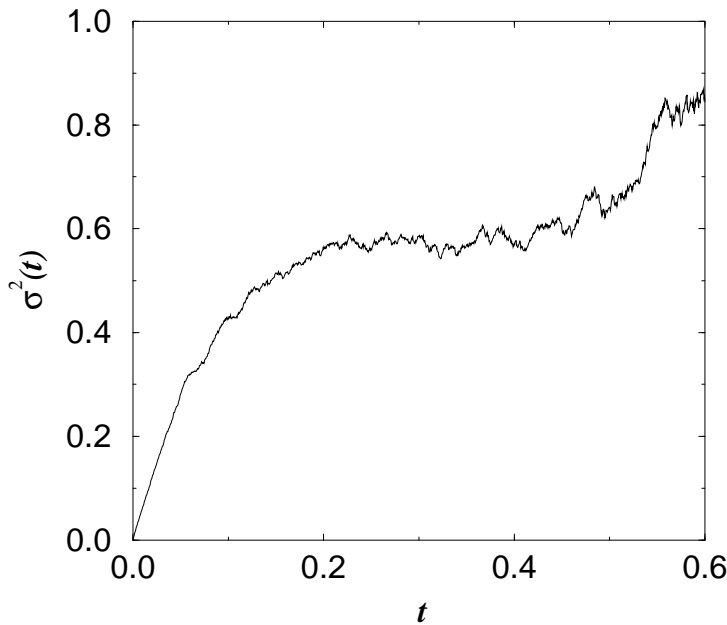


**Figure 6.** Variance of forcing functions for random waves inside the half-circle.

This is not surprising as the linear behaviour is predicted only for infinite curves. Curves closed to boundaries which do not exist in SLE require a special treatment which we will discuss in the next section. For short time when curves do not feel the boundary the variance is close to be linear.

In figure 7 the variance and the mean value are presented in a short interval of  $t$  where  $\sigma^2(t)$  is approximately linear. The solid line in this figure is the best quadratic fit to the variance

$$y = -0.003 + 6.05t - 10.0t^2 . \quad (14)$$

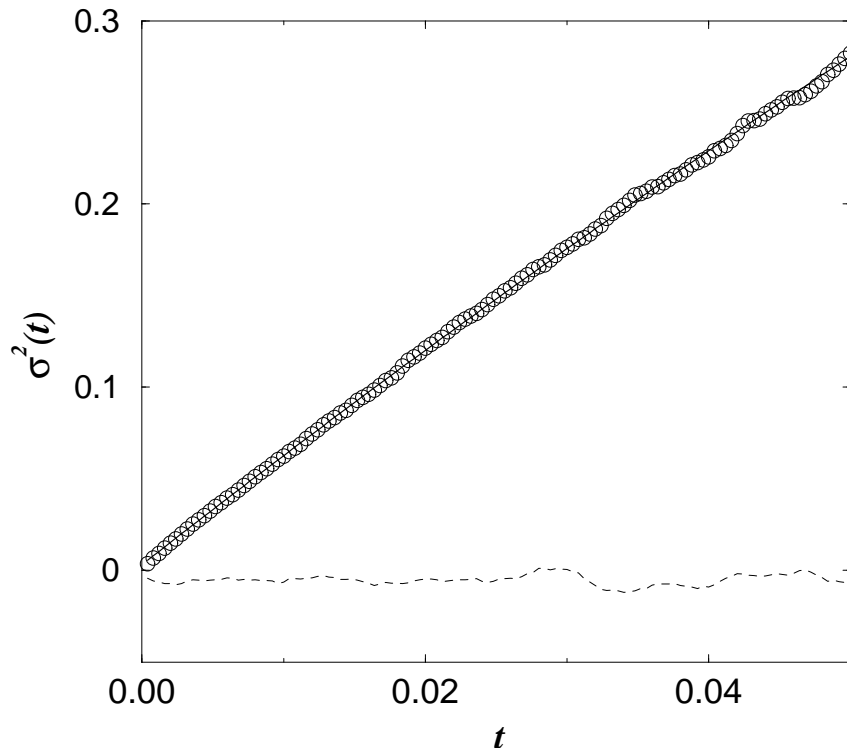


**Figure 7.** Variance (circles) and mean value (dashed line) in a short range. Solid line is the best quadratic fit (14).

The most important for us is the value of the linear term, 6.05. It is quite close to the pure percolation value  $\kappa = 6$ . The mean value of the forcing functions ( $\approx 0$ ) also agrees with the SLE value.

Another important prediction of the  $\text{SLE}_6$  description of the percolation model is that the distribution of values of  $\xi_t$  with fixed  $t$  has to be Gaussian with variance  $6t$ . In figure 8 this distribution is presented for different values of  $t$ . When the abscissa axis is rescaled by  $\sqrt{6t}$  all data are quite close to the Gaussian curve with unit variance. Similar results were obtained when instead of the half-circle we consider nodal lines inside a rectangle.

The agreement of our results with  $\text{SLE}_6$  predictions confirms that the nodal lines of random wave functions are well described by the percolation model, as was conjectured in [4].

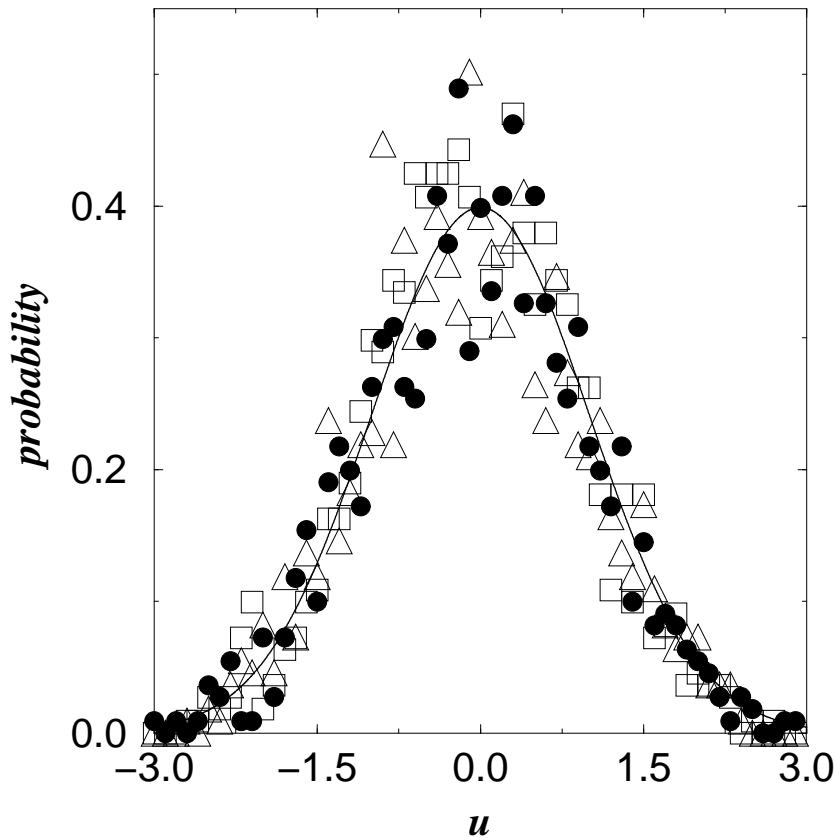


**Figure 8.** Probability law for random wave forcing functions. The abscissa axis is, as it follows for  $SLE_6$ ,  $u = \xi_t/\sqrt{6t}$ . The solid line is the standard Gaussian with unit variance:  $P(u) = \exp(-u^2/2)/\sqrt{2\pi}$ . The points indicated by  $\bullet$ ,  $\triangle$ , and  $\square$  correspond to, respectively,  $t = 0.02$ ,  $0.04$ , and  $0.06$ .

#### 4. Dipolar SLE

Though the results of the previous section are in a good agreement with  $SLE_6$ , let us notice two facts. First, the approximately linear increase of the variance with time is observed only for a very small time interval. Second, even within this interval a quadratic term in  $t$  always exists and is quite large (cf. (14)). Both of these drawbacks are related with inevitable finite size effects and can be reduced by the using of another variant of SLE.

The situation is analogous to the Brownian motion in a finite interval. It is well known (see e.g. [16]) that the probability for an one-dimensional Brownian particle starting from  $x_0$  to arrive to the point  $x$  at time  $t$  in the whole space is given by the Green function of the diffusion equation

$$G_0(x, x_0; t) = \frac{1}{\sqrt{2\pi Dt}} \exp\left(-\frac{(x - x_0)^2}{2Dt}\right) \quad (15)$$

where  $D$  is a diffusion coefficient. Standard relations  $\langle x \rangle = x_0$  and  $\langle (x - x_0)^2 \rangle = Dt$  are simple consequences of this expression.

For the Brownian motion inside a finite interval such probability depends on the boundary conditions. There are two main types of boundary conditions: reflecting and absorbing. When a particle hits a reflecting boundary it reflects back, when it touches an absorbing boundary it stops. It is known (see e.g. [16]) within the formalism of the diffusion equation that a reflecting boundary gives rise to the Neumann boundary condition and an absorbing one corresponds to the Dirichlet condition. When both boundaries of an interval of length  $h$  are of the same type one gets that the Green function of this interval is

$$G_{\pm}(x, x_0; t) = \sum_{m=-\infty}^{\infty} (G_0(x + 2mh, x_0; t) \pm G_0(-x + (2m + 1)h, x_0; t)) \quad (16)$$

Here  $+$  (resp.  $-$ ) denote Neumann (resp. Dirichlet) boundary conditions imposed at points  $\pm h/2$ .

In figure 9 the mean variance

$$\sigma^2(t) = \int_{-h/2}^{h/2} (x - \bar{x})^2 G_{\pm}(x, x_0; t) dx \quad (17)$$

is plotted as a function of  $t$  for the case  $x_0 = 0$  and  $D = 1$ . It is clearly seen that the long time behaviour depends on the boundary conditions and that the variance is linear in  $t$  only for very small  $t$ . These curves are similar to figure 6 where the linear

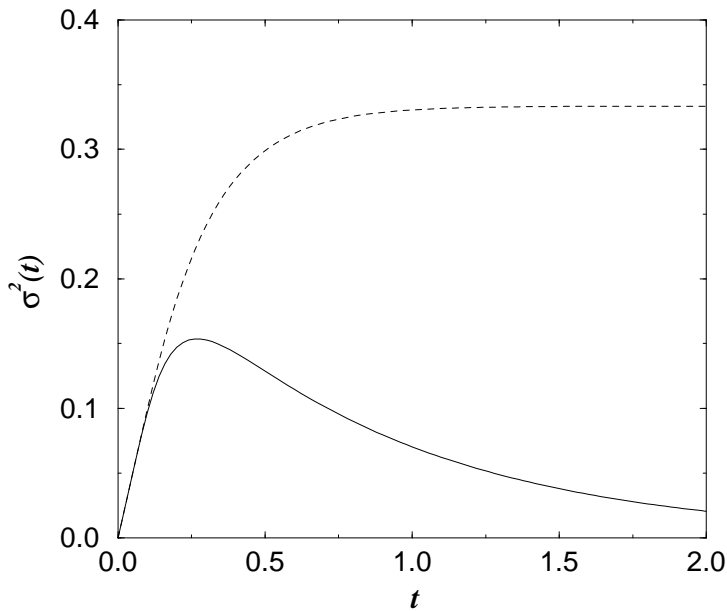


**Figure 9.** Variance for the one-dimensional Brownian motion with absorbing boundaries (solid line) and reflecting ones (dashed line).

behaviour was observed only for  $t < 0.05$  (cf. figure 7). We estimated that in the best cases this interval corresponds to, roughly speaking, only 1/4 of the total curve length.

To take into account larger parts of the curves and to check the Brownian-type behaviour for a longer time interval it is required to construct formulae similar to (16) for SLE.

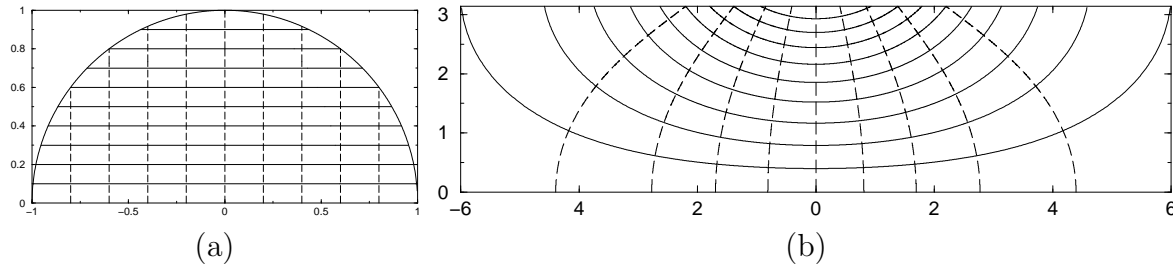


**Figure 10.** (a) Rectangular lattice inside the half-circle. (b) Its image under the map (20).

The simplest case corresponds to the reflecting boundary conditions. In this setting one considers a region and random curves (nodal lines) which start at one fixed point,  $z_0$ , of the boundary and end at another fixed boundary point,  $z_1$ . For the nodal lines this can be achieved e.g. by imposing that one boundary arc from  $z_0$  to  $z_1$  is positive and the second one is negative. This type of processes is called chordal SLE (see e.g. [13]). By definition, it can be reduced to the standard SLE from 0 to infinity (cf. (9)) by a conformal transformation which transforms the given region to the upper half plane in such a way that the point  $z_0$  is mapped to the origin and the point  $z_1$  to infinity.

Here, we would like to use a different variant of SLE which corresponds to a region with two boundary arcs restricted by points  $z_+$  and  $z_-$ . One arc is assumed to be a reflecting boundary and the other is an absorbing boundary. The random curves emerge from the point  $z_0$  on the reflecting boundary and are stopped when they hit the absorbing arc. By a conformal transformation our region can be transformed to the standard strip  $\mathbb{S}$

$$\mathbb{S} = \{z \in \mathbb{C}, 0 < \text{Im } z < \pi\} \quad (18)$$

in such a way that points  $z_-$ ,  $z_+$ , and  $z_0$  are mapped to  $-\infty$ ,  $+\infty$ , and 0 respectively.

In [10] it was shown that the  $\text{SLE}_\kappa$  process which joins 0 to a point of the line  $\text{Im } z = \pi$  is described by the following Loewner-type equation

$$\frac{dg_t(z)}{dt} = \frac{2}{\tanh(g_t(z) - \xi_t)} \quad (19)$$

where  $g_0(z) = z$  and the forcing function,  $\xi_t$ , is as above the standard Brownian motion (12) with variance  $\kappa t$ .

To construct the dipolar SLE numerically from the data used in the previous section we first transform the nodal lines inside the half-circle, as in figure 3, to the standard strip (18) by the following transformation

$$F(z) = \ln[(L+z)^2/(L-z)^2] \quad (20)$$

where  $L$  is the circle radius.

To visualize this mapping we present the images of a rectangular lattice inside the half-circle in figure 10. Note the strong deformations of the regions close to the absorbing boundary.

The first step of calculations consists in the transformation of every nodal lines inside the half-circle to lines inside the chosen strip (18). Such an example is illustrated in figure 11.

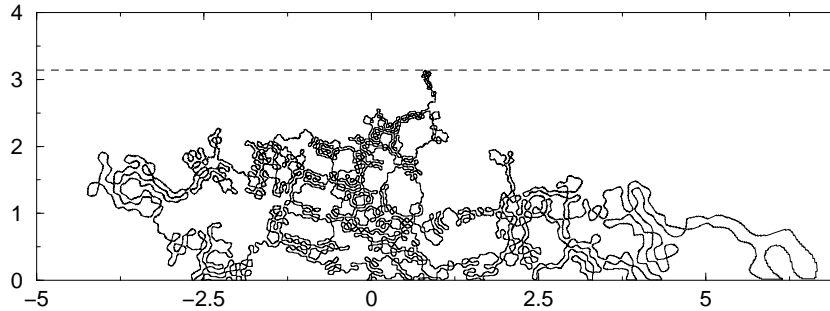


**Figure 11.** Image of the nodal line of figure 3 under the map (20). The dashed line is the absorbing boundary.

Then it is necessary to find the dipolar conformal transformation which map the strip with a line to the strip itself (cf. (19)). In the appendix a simple algorithm for such a mapping is briefly discussed. Using it we compute numerically the forcing function,  $\xi_t$  for each nodal line and calculate its statistical properties. In figure 12 the variance (13) is plotted for all curves and in figure 13 the region of linear increase of  $\sigma^2(t)$  is

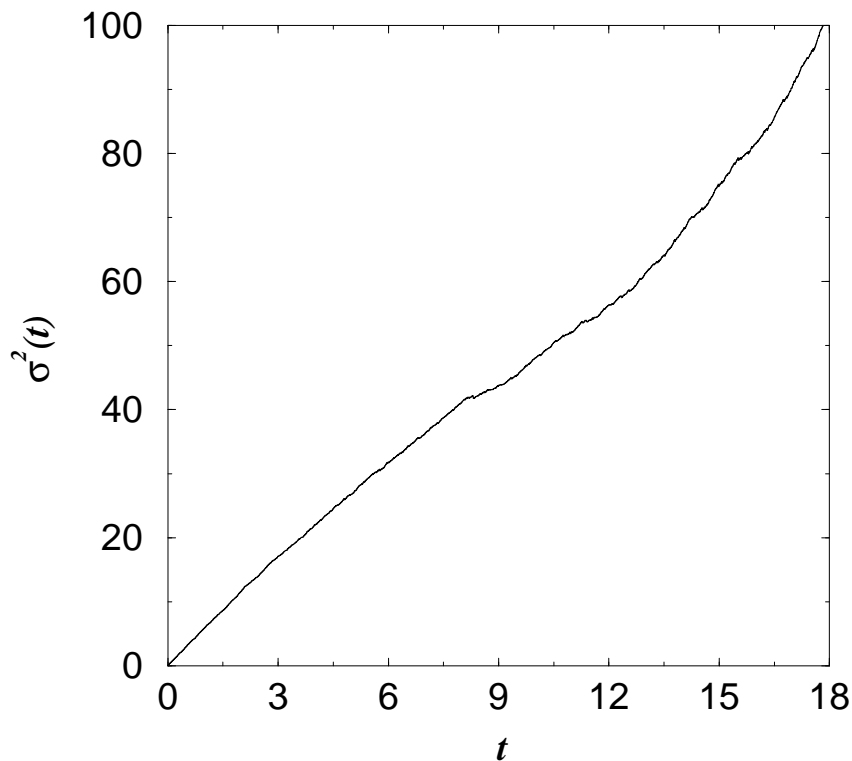


**Figure 12.** Variance of forcing functions for the nodal lines inside the strip.

magnified. The solid line in this figure indicates the best quadratic fit

$$y = 5.92t - 0.103t^2 . \tag{21}$$

The coefficient 5.92 is to compare with the percolation theory value of  $\kappa = 6$ . Other statistical characteristics are also in a good agreement with the  $SLE_6$  predictions.

Contrary to (14) the quadratic term in (21) is small. It is mainly related with discretization errors and it decreases when more points along a curve are taken into account. The non-linear behaviour of the variance in figure 12 for large  $t$  is connected with large errors due to the stretching of lines close to the boundary as it is evident from figures 10 and 11. We checked that the interval  $t < 8$  in figure 13 where the variance is linear in  $t$  corresponds approximately to 92% of the total curve length. It means that the dipolar  $SLE_6$  is a good description of the nodal lines practically for the entire curves. Exceptions are the small line parts close to the absorbing boundary which require better approximations.

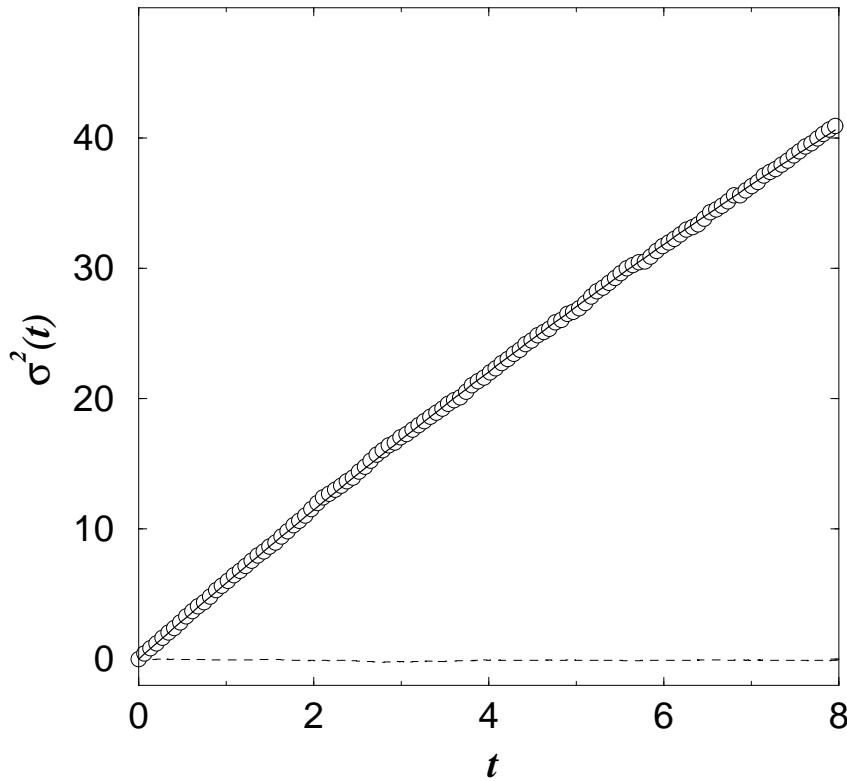


**Figure 13.** Variance (circles) and mean value (dashed line) for 2252 realizations inside the strip. Solid line: the best fit (21).

We have also investigated nodal lines inside a rectangle  $[-L/2; L/2] \times [0; l]$  which can be conformally mapped into the strip (18) by the following transformation

$$F(z) = -\ln[(\wp(z + L/2) - \wp(L))/(\wp(L/2) - \wp(L))] \tag{22}$$

where  $\wp(z)$  is the Weierstrass elliptic function with periods  $2L$  and  $2il$  (see e.g. [17]).

The results in this case are similar to the ones above and all agree well with the percolation model.

## 5. Conclusions

In summary, we investigated the nodal lines of two-dimensional random wave functions by numerically computing one-dimensional forcing functions of Loewner's evolution. We demonstrate that the later are well described by a Brownian motion with zero mean and variance growing linearly in time. The coefficient of proportionality is close to the value 6 predicted by the percolation model. Our results give an additional support to the conjecture that the nodal domains of random wave functions in the scaling limit are described by the critical percolation. We show that using dipolar SLE reduces significantly finite size effects.

## Acknowledgements

The authors are very thankful to J. Keating and I. Williams for useful discussions and, in particular, for pointing out an error in the calculations. One of the authors, E.B., is grateful to G. Falkovich for a discussion of the paper [5] prior the publication and to D. Bernard for clarifying discussions about SLE.

## Appendix

Consider a simple curve which starts on the real axis and grows inside a region of the upper half plane. The goal of the numerical algorithms below is to find a forcing function in (9) corresponding to a conformal map which transforms the region cut along the curve into the region itself.

Let  $(x_0, 0)$  be coordinates of the first point of the curve which we assume belongs to the abscissa axis and let  $(x_1, y_1)$  be coordinates of the next point closest to the first. The simplest numerical method consists of assuming that the forcing function is a piecewise constant function. The map with a constant forcing function  $\delta\xi$  for  $0 < t \leq \delta t$  is given by (6) as

$$g_t(z) = \delta\xi + \sqrt{(z - \delta\xi)^2 + 4\delta t}. \quad (23)$$

The parameters  $\delta\xi$  and  $\delta t$  are obtained from the condition that the top of the slit coincides with the point  $\delta z = x_1 - x_0 + iy_1$ , which yields

$$\delta\xi = \operatorname{Re} \delta z, \quad \delta t = \frac{1}{4}(\operatorname{Im} \delta z)^2. \quad (24)$$

Then we transform all points of the curve except the first one by (23) with these values of parameters and renumber the resulting points. One repeats this process till the whole curve will be transformed. In [18] it is proved that such an algorithm converges for sufficiently small  $\delta t_j$  and  $\delta x_j$ .

In section 3 we used the more refined geodesic algorithm [15] in which one approximates a small part of the curve between two points, 0 and  $\delta z$ , by the geodesic

arc (a circle perpendicular to the real axis) passing through these points. Normalizing the map given in [15] such as to obey the convention (4) one gets the expression

$$g_t(z) = \frac{b^3}{\sqrt{b^2 + c^2} \sqrt{(bz/(b-z))^2 + c^2 - b^2 - c^2}} + \frac{2b^3 + 3bc^2}{2(b^2 + c^2)} \quad (25)$$

where

$$b = \frac{|\delta z|^2}{\mathcal{R}e \delta z}, \quad c = \frac{|\delta z|^2}{\mathcal{I}m \delta z}. \quad (26)$$

Direct calculations give that the time corresponding to  $\delta z$  and the value of the forcing function in this point are

$$\delta t = \frac{1}{4}(\mathcal{I}m \delta z)^2 + \frac{1}{8}(\mathcal{R}e \delta z)^2 \quad (27)$$

and

$$\delta \xi_t = \frac{3}{2} \mathcal{R}e \delta z. \quad (28)$$

When a point moves along a geodesic circle of diameter  $b$  the forcing function changes as follows

$$\xi_t = \frac{12t}{b + \sqrt{b^2 - 8t}} \quad (29)$$

and is practically linear for short time. Eqs. (25)–(28) define the geodesic algorithm.

To do some computations following dipolar SLE in Section 4 we use a piecewise constant approximation for the forcing function in (19). In this case one has the exact solution [10]

$$\cosh \left( \frac{1}{2}(g_t(z) - \delta \xi) \right) = e^{\delta t/2} \cosh \left( \frac{1}{2}(z - \delta \xi) \right). \quad (30)$$

Finding  $\delta t$  and  $\delta \xi$  from the condition that the curve tip coincides with  $\delta z$  one obtains

$$\delta \xi = \mathcal{R}e \delta z, \quad \exp \left( -\frac{1}{2} \delta t \right) = \cos \left( \frac{1}{2} \mathcal{I}m \delta z \right). \quad (31)$$

These expressions are the dipolar analog of Eqs. (24) and they permit to construct the simplest algorithm of numerical calculations for the dipolar case.

## References

- [1] Berry M V (1977) Regular and irregular semi classical wave functions *J. Phys. A: Math. Gen.* **10** 2083
- [2] Blum G, Gnutzmann S and Smilansky U (2002) Nodal domains statistics: a criterion for quantum chaos *Phys. Rev. Lett.* **88** 114101
- [3] Bogomolny E and Schmit C (2002) Percolation model for nodal domains of chaotic wave functions *Phys. Rev. Lett.* **88** 114102
- [4] Bogomolny E and Schmit C (2006) Random wave functions and percolation *in preparation*
- [5] Bernard D, Boffetta G, Celani A and Falkovich G (2006) Conformal invariance in turbulence *Nature* **2** 124
- [6] Stauffer D and Aharony A (1994) *Introduction to Percolation Theory* (Taylor and Fransis, London)
- [7] Smirnov S (2001) Critical percolation in the plane : conformal invariance, Cardy's formula, scaling limits *Acad. Sc. Paris* **I**, **333** 239

- [8] Löwner K (1923) Untersuchungen über schlichte konforme Abbildungen des Einheitskreises I *Math. Ann.* **89** 103
- [9] Schramm O (2000) Scaling limits of loops-erased random walks and uniform spanning trees *Israel J. Math.* **118** 221
- [10] Bauer M, Bernard D, and Houdayer J (2005) Dipolar stochastic Loewner evolution *J. Stat. Mech.* P03001
- [11] Keating J P, Marklof J and Williams I G (2006) Nodal domain statistics for quantum maps, percolation and stochastic Loewner evolution *Phys. Rev. Lett.* **97** 034101
- [12] Keating J P and Williams I G (2006) private communication
- [13] Cardy J (2005) SLE for theoretical physicists *Annals Phys.* **318** 81
- [14] Werner W (2004) *Random planar curves and Schramm – Loewner evolution* (Lectures Notes in Mathematics) **1840** p 107
- [15] Marshall D and Rohde S (2005) Convergence of the Zipper algorithm for conformal mapping <http://www.math.washington.edu/~marshall/preprints/zipper.pdf>
- [16] Feller W (1968) *An Introduction to Probability Theory and its Applications* (Wiley)
- [17] Erdélyi A (1955) *Higher Transcendental Functions*, vol 3 (Mc Graw-Hill, New York, Toronto, London)
- [18] Bauer R O (2003) Discrete Loewner evolution (*Preprint* arXiv: math.PR/0303119)